Available online at www.sciencedirect.com
ScienceDirect
Acta Materialia 56 (2008) 3338–3343
Acta MATERIALIA
www.elsevier.com/locate/actamat

Evaluating plastic flow properties by characterizing indentation size effect using a sharp indenter

Ju-Young Kim [a,*], Seung-Kyun Kang [b], Julia R. Greer [a], Dongil Kwon [b]

[a] *Materials Science, California Institute of Technology, Pasadena, CA 91125, USA*
[b] *Department of Materials Science and Engineering, Seoul National University, Seoul 151-744, Republic of Korea*

Received 6 December 2007; received in revised form 28 January 2008; accepted 5 February 2008
Available online 21 April 2008

Abstract

The strain-hardening exponent, used in describing the plastic flow properties of materials, is evaluated from the characteristic length in the indentation size effect (ISE). A linear relationship is found between the strain-hardening exponent and the log of the ISE characteristic length for Ni and SCM21 (structural steel) samples with different plastic pre-strain values. These results are explained through the Taylor dislocation hardening model and a representative stress–strain approach. A dimensionless function characterizing the plastic deformation using only parameters generally measurable by nanoindentation testing is also proposed. The feasibility of developing a unique dimensionless function is studied for 22 metals.

Keywords: Indentation size effect; Nanoindentation; Strain-hardening exponent; Plastic flow properties

1. Introduction

Nanoindentation testing has been used widely to measure the mechanical properties of materials at small scales, by which hardness and elastic modulus of materials are generally evaluated [1–8]. Hardness is a measure of the resistance of a material to plastic deformation, which is sometimes related to its flow stress. Tabor demonstrated the relation between hardness and yield strength [9], and the relation between hardness and flow stress at a representative strain beneath the indenter has been established by many experimental and finite-element method (FEM) simulation results [10–22]. The elastic modulus is also measured by nanoindentation techniques [2], and thus the mechanical properties of a material usually derived from the uniaxial tensile stress–strain curve can be evaluated by nanoindentation testing alone if the plastic flow properties are measured. Since the experimental procedure for nanoindentation is simple and nondestructive, and places no limits on the sample size and geometry, using nanoindentation to measure plastic flow properties has attracted much research interest [11–22].

A representative stress–strain approach has been proposed to measure the yield stress, ultimate tensile strength and strain-hardening exponent of metals by defining a representative stress and strain beneath a spherical indenter [11,12]. This approach exploited the idea that the various representative strain states induced in a material beneath a spherical indenter depend on the indentation depth. However, the value of using a spherical indenter at the nanometer scale is still a subject of some debate, since it is difficult to correlate the indentation size effect (ISE) with an indenter radius as well as indentation depth [23,24]. Jayaraman et al. proposed a way to measure plastic properties by fitting a constitutive equation to two different representative stress–strain points obtained by two sharp indenter geometries: Berkovich and cube-corner indenters [16]. While better results are expected when the plastic flow

* Corresponding author.
E-mail address: jyk@caltech.edu (J.-Y. Kim).

1359-6454/$34.00 © 2008 Acta Materialia Inc. Published by Elsevier Ltd. All rights reserved.
doi:10.1016/j.actamat.2008.02.049

curve is fitted to more representative stress–strain data measured by the various sharp indenters with different angles, the effectiveness of this technique is limited due to the many experiments required. Algorithms using FEM have also been proposed [13,14,17–22], and inverse analysis [18,19] shows that universal dimensionless functions are set up by many forward analyses, by which the indentation force–displacement curve is determined from the stress–strain curve using FEM simulations, and a material's stress–strain curve is determined inversely by inputting the parameters of the indentation force–displacement curve and indenter geometry into these dimensionless functions. These FEM simulation-based methods are, however, strongly dependent on the particular FEM simulation and dimensionless functions used. The experimental evaluation of plastic flow properties by nanoindentation testing using a single sharp indenter, as discussed here, thus offers clear advantages over existing techniques.

One of the key parameters representing plastic flow properties is the strain-hardening exponent, n, for those materials that obey the Hollomon equation, $\sigma = K\varepsilon^n$, where σ is the true stress, ε is the true strain and K is the strength coefficient [25]. Most materials show a linear dependence with the slope corresponding to the strain-hardening exponent when true tensile stress is plotted vs. strain on a log–log scale. The present work began by considering the possibility of a relationship between the strain-hardening exponent, n, and the ISE characteristic length, h^*. The ISE is an increase in hardness with decreasing indentation depth observed in numerous nanoindentation experiments [23,24,26–45]. It is believed to be associated with the geometrically necessary dislocations (GNDs) induced by an inhomogeneous plastic deformation. Nix and Gao analyzed the ISE in crystalline materials by calculating the density of GNDs around a sharp indenter based on a Taylor dislocation hardening model [27]; Gao et al. and Huang et al. reformulated the mechanism-based strain gradient plasticity [29,30], and Swadener et al. extended the Nix–Gao model to a spherical indenter, taking the indenter's geometry as a parabola [23]. Although the presence of local strain gradients producing a higher GND density is the key explanation for the ISE, while any increase in strength during uniaxial deformation is caused by homogeneous hardening from an increase in the density of statistically stored dislocations (SSDs), Elmustafa et al. verified, by analyzing trends in the activation volume with hardness, that the ISE is driven by the same dislocation mechanisms as strain hardening [36].

This work examines the relationship between the strain-hardening exponent and the ISE characteristic length. We perform interrupted uniaxial tensile tests on Ni and SCM21 (structural steel), and thus obtain different values of the strain-hardening exponent by intentional plastic pre-strain. The values of ISE characteristic lengths were measured by nanoindentation using a Berkovich indenter. The experimentally determined relationship between the strain-hardening exponent and the ISE characteristic length is analyzed via a Taylor dislocation hardening model and the representative stress–strain approach. We report this relationship for 22 different metals.

2. Experiments

The strain-hardening exponents of samples were intentionally controlled by interrupted tensile tests. Uniaxial tensile tests were performed on pure polycrystalline Ni and SCM21 at a displacement rate of 1 mm min^{-1} until necking occurred. On the basis of the stress–strain curve, tensile tests were interrupted at true strain values of 5%, 10% and 15% for Ni, and 2% and 5% for SCM21. The uniformly deformed gauge sections were cut and gently polished up to 0.3 μm alumina powder. Nanoindentation tests were conducted on undeformed and 5%, 10% and 15% pre-deformed Ni samples, as well as on undeformed and 2% and 5% pre-deformed SCM21 samples. The continuous stiffness measurement (CSM) technique of the Nanoindenter XP (MTS Inc., TN, USA) using a three-sided pyramidal Berkovich indenter was used in all nanoindentation tests. The loading/unloading rate was constant at 0.2 mN s^{-1}; the maximum load was 100 mN, and a drift rate below 0.05 nm s^{-1} was allowed. To establish the relationship between the strain-hardening exponent and the ISE characteristic length, 22 metals were subjected to uniaxial tensile tests and nanoindentation tests under the conditions described above. The samples were general structural steels (S45C, SKD11, SKH9, SKS3, SKD61, SCM4), cast irons (CI300, CI600), stainless steels (STS 303, STS 304, STS 316L), API X-grade steels (API X65, X70, X80), Ti alloys (pure Ti, Ti–6Al–6V, Ti–5Al–2.5Sn, Ti–10V–2Fe–3Al), Al alloys (Al2011, Al6061, Al7076) and pure polycrystalline Cu. Their elastic moduli, Poisson's ratios and shear moduli were measured by an ultrasonic pulse-echo technique using a two-channel digital real-time oscilloscope for the theoretical calculation of the representative stress induced by nanoindentation.

3. Results and discussion

Fig. 1 shows the tensile true stress–strain curves for undeformed Ni and SCM21; the strain-hardening exponents n and strength coefficients K of undeformed and pre-deformed samples are presented in Table 1. These values were calculated from the uniaxial stress–strain curves of undeformed samples by assuming that the stress–strain curves of pre-deformed samples have constant elastic modulus during unloading and reloading. The true stress–strain curves of undeformed Ni and SCM21 samples were found to be described well by the Hollomon equation. The strain-hardening exponent n was found to decrease and the strength coefficient K to increase with increasing plastic pre-strain. Fig. 2 shows the hardness variation with indentation depth. ISE characteristic lengths were calculated by using the Nix–Gao model:

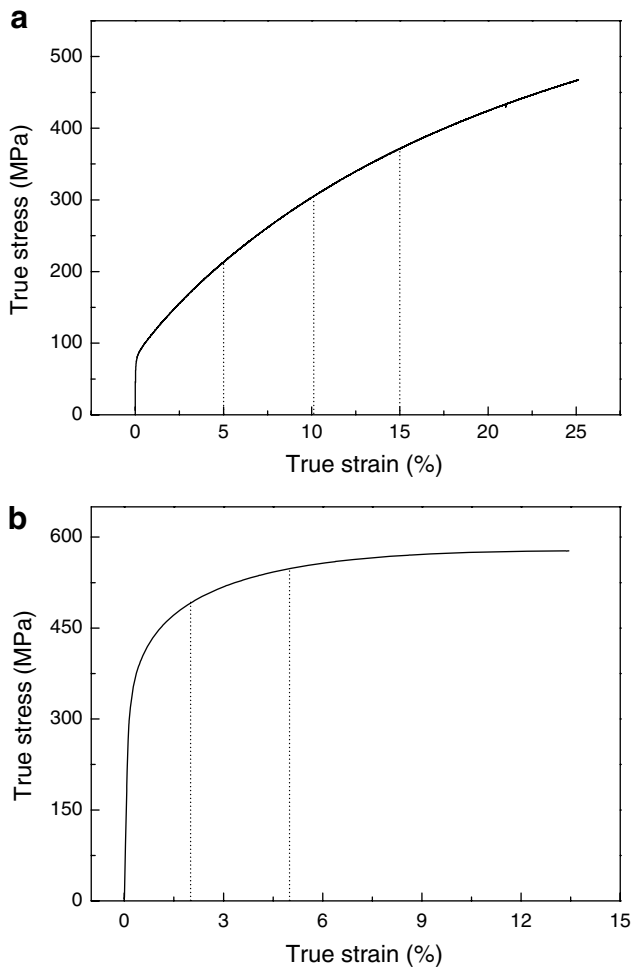

Fig. 1. Uniaxial tensile stress–strain curves of undeformed (a) Ni and (b) SCM21.

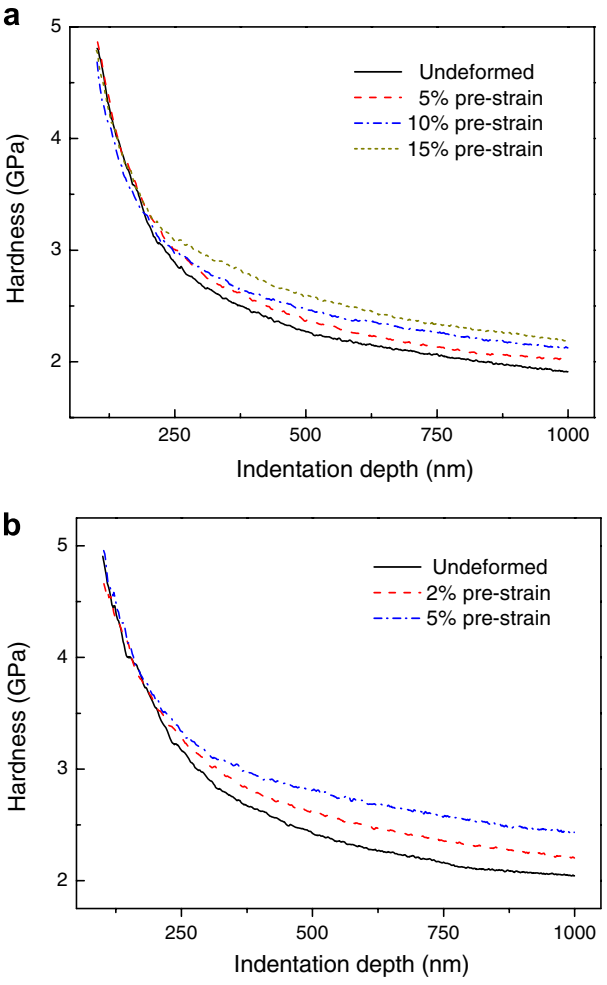

Fig. 2. Hardness vs. indentation depth for (a) Ni and (b) SCM21.

$$\frac{H}{H_0} = \sqrt{1 + \frac{h^*}{h}} \tag{1}$$

where H is the hardness, H_0 is the macroscopic hardness and h is the indentation depth (also shown in Table 1) [27]. Note that ISE can be seen to be stronger in Fig. 2 than the measured values in Table 1 simply because the sample used in Fig. 2 had a shallower indentation depth than that featuring in other studies [27,28,44]. Hardness values measured at indentation depths greater than 200 nm were used to characterize the indentation size effect to alleviate the effect of the work-hardened layer formed by mechanical polishing [31]. The macroscopic hardness H_0 was found to increase and the ISE characteristic length h^* to decrease with increasing plastic pre-strain. The macroscopic hardness and ISE characteristic length in the Nix–Gao model are given by

Table 1
Parameters measured from uniaxial tensile stress–strain curves and characterized for ISE, and theoretically calculated flow stress and strain-hardening exponent values

Material	Ni				SCM21		
Plastic pre-strain (%)	0	5	10	15	0	2	5
n	0.452	0.211	0.117	0.062	0.151	0.072	0.035
K (MPa)	864.14	601.84	541.68	511.53	902.66	751.36	702.97
h^* (nm)	812.29	628.25	549.76	516.41	811.95	538.47	454.28
H_0 (GPa)	1.339 (± 0.039)	1.506 (±0.062)	1.709 (±0.072)	1.819 (±0.065)	1.468 (±0.079)	1.719 (±0.094)	1.873 (±0.117)
Flow stress at 7% true strain (MPa)	252.48	331.43	392.48	440.72	563.47	570.82	576.46
Representative stress calculated from h^* (MPa)	506.35	575.76	615.49	635.05	550.89	676.46	736.49
Calculated n using Eq. (5)	0.203	0.017	−0.048	−0.082	0.206	0.059	0.001

$$H_0 = 3\sqrt{3}\alpha\mu b\sqrt{\rho_s} \tag{2a}$$

$$h^* = \frac{81}{2} b\alpha^2 \tan^2\theta \left(\frac{\mu}{H_0}\right)^2 \tag{2b}$$

where α is a geometric constant, μ is the shear modulus, b is the magnitude of the Burgers vector, ρ_s is the density of SSDs and θ is the complementary angle of the conical indenter half-angle (19.7° for the Berkovich indenter). In the Nix–Gao model, the von Mises flow rule applies and a Tabor factor of 3 is used to convert the flow stress to hardness. An increase in the plastic pre-strain produces a higher SSD density, which is manifested by the strain-hardening behavior and leads, via Eq. (2a), to an increase in the macroscopic hardness. Since all the parameters in Eq. (2b) except for the macroscopic hardness are insensitive to the plastic pre-strain, the ISE characteristic length is the only factor that must decrease in response to an increase in the plastic pre-strain.

The strain-hardening exponent and log value of the ISE characteristic length normalized by the Burgers vector (0.25 nm for Ni and 0.248 nm for SCM21) are remarkably linear for each material, as shown in Fig. 3. The deformation state of the material underneath the sharp indenter is defined by the representative stress and strain, which is identified with the point on the true stress–strain curve obtained via a uniaxial tensile test. The representative stress σ_r can also be described by the Hollomon equation

$$\sigma_r = K\varepsilon_r^n \tag{3}$$

where ε_r is the representative strain induced by nanoindentation. In particular, assuming that the Taylor dislocation hardening model and the von Mises flow rule apply, as assumed by the Nix–Gao model, we also have

$$\sigma_r = \sqrt{3}\alpha\mu b\sqrt{\rho_s} \tag{4}$$

where σ_r is the representative flow stress at a representative strain ε_r, a function of indenter geometry. Representative strain is defined by Johnson as $0.2 \cdot \cot\theta$, corresponding to 0.07 for the Berkovich indenter [10]. Therefore, the flow stress values at 7% true strain were measured from the uniaxial tensile stress–strain curves, and the representative stress values in nanoindentation by the Berkovich indenter were subsequently calculated from Eq. (4) by using the experimentally measured shear modulus, ISE characteristic length, and $\alpha = 0.5$. Table 1 shows the relatively good agreement between the measured and calculated flow stress values when taking into consideration the geometric constant α, which is known to be a constant with value from 0.3 to 0.6. Equating Eqs. (3) and (4) and converting them to dimensionless format by using Eqs. (2a) and (2b) yields the following expression for the strain-hardening exponent

$$n = -\frac{1}{2\ln\varepsilon_r}\ln\left(\frac{h^*}{b}\right) - \frac{1}{\ln\varepsilon_r}\ln\left(\frac{K}{\mu}\right) + \frac{1}{\ln\varepsilon_r} \times \ln\left(\frac{3}{\sqrt{2}}\alpha\cot\theta\right) \tag{5}$$

Here the representative strain ε_r is a function of indenter geometry, i.e. it is constant for a self-similar sharp indenter. Therefore, the relationship between n and $\ln(h^*/b)$ is linear unless the other two terms interrupt the linear relationship. Eq. (5) also suggests that n can be evaluated from h^* when the material parameters, b, K, μ, and α, and the indenter geometry θ are known. Since the undeformed and pre-deformed samples have the same values of b, μ, α and θ; only K is changed by the plastic pre-strain, as shown in Table 1. Consequently, the third term in Eq. (5) does not vary with the strain-hardening exponent, and the second term can alter the linear relationship between n and $\ln(h^*/b)$.

Fig. 4 shows the relationship between the dimensionless terms corresponding to the ISE characteristic length h^* (first dimensionless term in Eq. (5)) and the strength coefficient K (second term in Eq. (5)). The linear relationship between these two dimensionless terms indicates that the strain-hardening exponent n can be described by a linear function of $\ln(h^*/b)$ in Eq. (5). The ISE characteristic

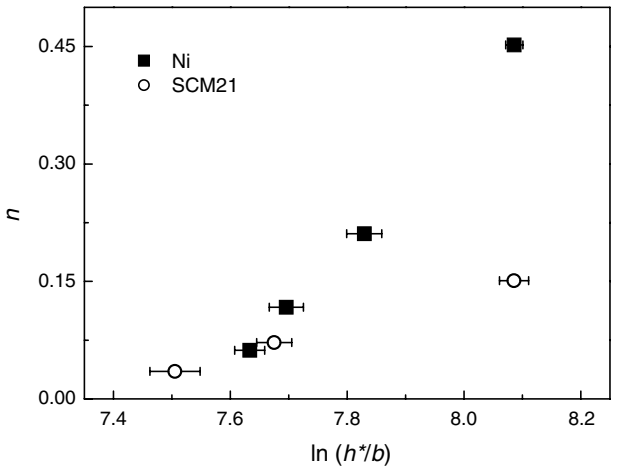

Fig. 3. Strain-hardening exponent n vs. log of ISE characteristic length normalized by Burgers vector (log (h^*/b)) for Ni and SCM21.

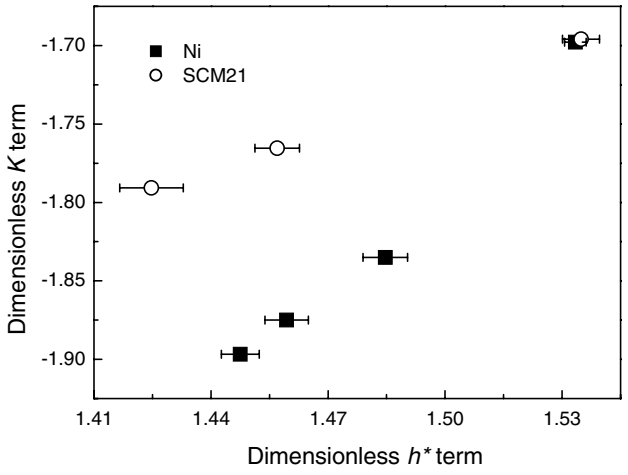

Fig. 4. Dimensionless term corresponding to the strength coefficient $\ln(K/\mu)$ vs. the term corresponding to ISE characteristic length $\ln(h^*/b)$ in Eq. (5).

length h^* is proportional to the inverse square of the macroscopic hardness H_0 in Eq. (2b), since the other parameters in Eq. (2b) are insensitive to the plastic pre-strain. The macroscopic hardness can be converted to a representative stress σ_r by using Eq. (4). Equating the macroscopic hardness and representative stress $H_0/3 = K\varepsilon_r^n$ and rearranging terms by using the log and linear relationship between n and $\ln(h^*/b)$ leads easily to the linear relationship between $\ln(h^*/b)$ and $\ln(K/\mu)$. In addition, the revision of the Nix–Gao model in Ref. [44], in which storage volume of GNDs was corrected by multiplying proportionality factor, leading to smaller h^*, does not change the basic linear relationship in Eq. (5).

If the strain-hardening exponent n can be described by $\ln(h^*/b)$, as shown above, it would be very useful in analyzing the plastic deformation induced by nanoindentation, as well as in evaluating the strain-hardening exponent by a general nanoindentation test. The true stress–strain behavior of a material is assumed to be

$$\sigma = \begin{cases} E\varepsilon, & \varepsilon \leqslant \varepsilon_y \\ K\varepsilon^n, & \varepsilon \geqslant \varepsilon_y \end{cases} \tag{6}$$

where ε_y is the yield strain. In trying to obtain a quantitative mechanical response, the deformation induced by introducing a sharp indenter into a material can be described by a dimensionless function Π

$$\Pi = \Pi(E_r, \varepsilon_y, n, \theta) \tag{7}$$

where E_r is the reduced elastic modulus given by

$$E_r = \left(\frac{1-\nu^2}{E} + \frac{1-\nu_i^2}{E_i}\right)^{-1} \tag{8}$$

where E_i and ν_i are the elastic modulus and Poisson's ratio of the indenter. E_i, ν_i and ν are generally known, and the elastic modulus of a material can be evaluated from the measured reduced elastic modulus. In nanoindentation, the yield strain (second parameter in Eq. (7)) is related to the portion of elastic strain at a given total (representative) strain that is independent of indentation depth for a sharp indenter because of its self-similarity. This parameter can be inferred from a variety of sources, for instance the ratio of yield strength to elastic modulus σ_y/E, the ratio of hardness to elastics modulus H/E, the ratio of final indentation depth to maximum indentation depth h_f/h_{max} and the ratio of work recovered during elastic unloading to total work input during loading $W_{elastic}/W_{total}$ [13,14,16–22,46–52]. If the strain-hardening exponent is evaluated from the ISE characteristic length, as described above, and the angle of the sharp indenter is given, the plastic deformation induced by nanoindentation can be determined by relying only on those parameters measurable in nanoindentation tests as

$$\Pi = \Pi(E_r, \varepsilon_y, n, \theta) = \Pi_\theta\left(E_r, \frac{W_{elastic}}{W_{total}}, \ln\left(\frac{h^*}{b}\right)\right) \tag{9}$$

Fig. 5 shows the relationship between the ISE characteristic length and strain-hardening exponent for the 22 different metals, including general structural steels, cast irons, stainless steels, API X-grade steels, titanium alloys, aluminum alloys and pure polycrystalline copper. While some scatter is present in the data, it is clear that most metals show a linear dependence of the log of ISE characteristic length normalized by the Burgers vector and the strain-hardening exponent. Note that a linear relation between n and $\ln(h^*/b)$ is obtained only when $\ln(h^*/b)$ and $\ln(K/\mu)$ have a linear relationship, as in the controlled plastic pre-strain situation. A roughly linear dependence between n and $\ln(h^*/b)$ for the randomly selected 22 metals might arise from the generally lower strain hardening exponent and lower ISE characteristic length of higher-strength materials. This result shows the feasibility of developing a unique dimensionless function describing the relationship between n and $\ln(h^*/b)$ for specific materials.

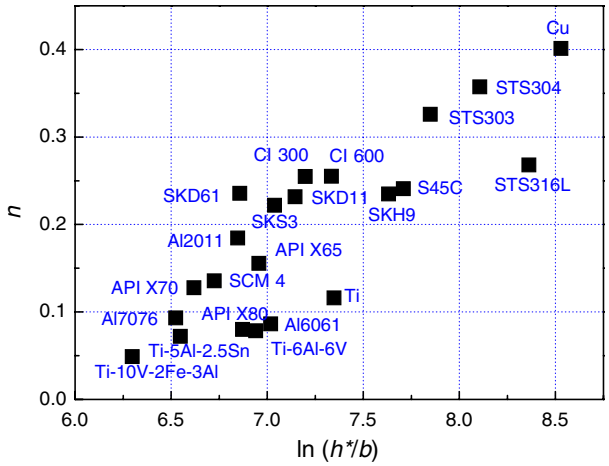

Fig. 5. Strain-hardening exponent n vs. log values of ISE characteristic length normalized by magnitude of Burgers vector $\ln(h^*/b)$ for various metals.

4. Conclusions

Strain-hardening exponents and ISE characteristic lengths of Ni and SCM21 with different plastic pre-strain were measured and analyzed. A linear relationship between the strain-hardening exponent and the log of the ISE characteristic length normalized by the Burgers vector was found. This is analyzed by using the Taylor dislocation hardening model and the representative stress–strain approach. We showed that a linear relationship between n and $\ln(h^*/b)$ is achieved when the relationship between $\ln(h^*/b)$ and $\ln(K/\mu)$ is linear, as is the case in the samples with different plastic pre-strain. On the basis of results from 22 different metals and alloys, a dimensionless function using the relationship between the strain-hardening exponent and ISE characteristic length was proposed to describe plastic deformation by nanoindentation with a sharp indenter. A clear correlation between the strain-hardening exponent and the ISE characteristic length means that the material deformation induced by nanoindentation with a sharp indenter can be fully described by using only parameters measurable through nanoindentation

tests. This result is significant in the determination of nanoindentation related plastic flow properties, such as pile-up/sink-in and plastic zone size. As an application of this result, we are currently working on correlating the nanoindentation derived and conventional hardness values by measuring the contact depth in the loaded state from the ISE characteristic length.

Acknowledgement

This work was supported by the Korea Research Foundation Grant (KRF-2007-357-D00138) funded by the Korean Government (MOEHRD).

References

[1] Doerner MF, Nix WD. J Mater Res 1986;1:601.
[2] Oliver WC, Pharr GM. J Mater Res 1992;7:1564.
[3] Oliver WC, Pharr GM. J Mater Res 2004;19:3.
[4] Cheng YT, Cheng CM. Mater Sci Eng R 2004;44:91.
[5] Gouldstone A, Chollacoop N, Dao M, Li J, Minor AM, Shen YL. Acta Mater 2007;55:4015.
[6] Fischer-Cripps AC. Vacuum 2000;58:569.
[7] Mukhopadhyay NK, Paufler P. Int Mater Rev 2006;51:209.
[8] Schuh CA. Mater Today 2006;9(5):32.
[9] Tabor D. Hardness of metals. OX: Clarendon Press; 1951.
[10] Johnson KL. Contact mechanics. CA: Cambridge University Press; 1985.
[11] Ahn JH, Kwon D. J Mater Res 2001;16:3170.
[12] Kim JY, Lee KW, Lee JS, Kwon D. Surf Coat Tech 2006;20:4278.
[13] Taljat B, Zacharia T, Kosel F. Int J Solids Struct 1998;35:4411.
[14] Dao M, Chollacoop N, Van Vliet KJ, Venkatech TA, Suresh S. Acta Mater 2001;49:3899.
[15] Herbert EG, Pharr GM, Oliver WC, Lucas BN, Hay JL. Thin Solid Films 2001;398–399:331.
[16] Jayaraman S, Hahn GT, Oliver WC, Rubin CA, Bastias PC. Int J Solids Struct 1998;35:365.
[17] Cheng YT, Cheng CM. Int J Solids Struct 1999;36:1231.
[18] Chollacoop N, Dao M, Suresh S. Acta Mater 2003;51:3713.
[19] Giannakipoulos AE, Suresh S. Scripta Mater 1999;40:1191.
[20] Venkatesh TA, Van Vliet KJ, Giannakopoulos AE, Suresh S. Scripta Mater 2000;42:833.
[21] Bucaille JL, Stauss S, Felder E, Michler J. Acta Mater 2003;51:1663.
[22] Bouzakis KD, Michailidis N. Thin Solid Films 2004;469–470:227.
[23] Swadener JG, George EP, Pharr GM. J Mech Phys Sol 2002;50:681.
[24] Qu S, Huang Y, Pharr GM, Hwangg KC. Int J Plasticity 2006;22:1265.
[25] Hollomon JH. Trans AIME 1945;162:268.
[26] Ma Q, Clarke DR. J Mater Res 1995;10:853.
[27] Nix WD, Gao H. J Mech Phys Sol 1998;46:411.
[28] McElhaney KW, Vlassak JJ, Nix WD. J Mater Res 1998;13:1300.
[29] Gao H, Huang Y, Nix WD, Hutchinson JW. J Mech Phys Sol 1999;47:1239.
[30] Huang Y, Gao H, Nix WD, Hutchinson JW. J Mech Phys Sol 2000;48:99.
[31] Liu Y, Ngan AHW. Scripta Mater 2001;44:237.
[32] Qiu X, Huang Y, Nix WD, Hwang KC, Gao H. Acta Mater 2001;49:3949.
[33] Tymiak NI, Kramer DE, Bhar DF, Wyrobek TJ, Gerberich WW. Acta Mater 2001;49:1021.
[34] Swadener JG, George EP, Pharr GM. J Mech Phys Sol 2002;50:681.
[35] Gao H, Huang Y. Scripta Mater 2003;48:113.
[36] Elmustafa AA, Stone DS. J Mech Phys Sol 2003;51:357.
[37] Qu S, Huang Y, Nix WD, Jiang H, Zhang F, Hwang KC. J Mater Res 2004;19:11.
[38] Feng G, Nix WD. Scripta Mater 2004;51:599.
[39] Zhang TY, Xu WH, Zhao MH. Acta Mater 2004;52:57.
[40] Wei Y, Wang X, Zhao M. J Mater Res 2004;19:208.
[41] Kim JY, Lee BW, Read DT, Kwon D. Scripta Mater 2005;52:353.
[42] Kim JY, Lee JJ, Lee YH, Jang JI, Kwon D. J Mater Res 2006;21:2975.
[43] Kim JY, Kang SK, Lee JJ, Jang JI, Lee YH, Kwon D. Acta Mater 2007;55:3555.
[44] Durst K, Backes B, Franke O, Göken M. Acta Mater 2006;54:2547.
[45] Huang Y, Zhang F, Hwang KC, Nix WD, Pharr GM, Feng G. J Mech Phys Sol 2006;54:1668.
[46] Cheng YT, Li Z. Philos Mag A 2002;82:1821.
[47] Chnge YT, Cheng CM. Appl Phys Lett 1998;73:614.
[48] Malzbender J, De With G. J Mater Res 2002;17:502.
[49] Pharr GM, Bolshakov. J Mater Res 2002;17:2660.
[50] Bolshakov A, Pharr GM. J Mater Res 1998;13:1049.
[51] Hay JC, Bolshakov A, Pharr GM. J Mater Res 1999;14:2296.
[52] Joslin DL, Oliver WC. J Mater Res 1990;5:123.